https://doi.org/10.5194/egusphere-2025-2656
Preprint. Discussion started: 25 August 2025


# Assessing the ability of the ECMWF seasonal prediction model to forecast extreme September-to-November rainfall events over Equatorial Africa

**Hermann N. Nana[1*] · Roméo S. Tanessong[2,1] · Masilin Gudoshava[3] · Derbetini A. Vondou[1]**

[1]Laboratory for Environmental Modelling and Atmospheric Physics (LEMAP), Physics Department, University of Yaounde 1, PO Box 812, Yaounde (Cameroon)

[2]Department of Meteorology and Climatology; Higher Institute of Agriculture, Forestry, Water and Environment; University of Ebolowa, PO Box 118, Ebolowa (Cameroon)

[3]IGAD Climate Prediction and Applications Centre (ICPAC), Nairobi, (Kenya)

* Corresponding author: Hermann N. Nana (nanahermann100@yahoo.com)

Hermann N. Nana's orcid: https://orcid.org/0000-0002-0973-8613

Roméo S. Tanessong's orcid: https://orcid.org/0000-0003-3804-5901

Masilin Gudoshava's orcid: https://orcid.org/0000-0003-0315-9271

Derbetini A. Vondou's orcid: https://orcid.org/0000-0002-8681-5328

https://doi.org/10.5194/egusphere-2025-2656
Preprint. Discussion started: 25 August 2025


## Abstract

This study investigates the predictability of rainfall over Equatorial Africa (EA) and evaluates the forecasting performance of the European Centre for Medium-Range Weather Forecasts fifth-generation seasonal forecast version 5.1 (ECMWF-SEAS5.1) for the September–November (SON) periode during 1981–2023 (43 years). The analysis considers two lead-times, focusing on initial conditions (ICs) from September and August. Regression, spatiotemporal and composite analyses are applied to highlight the relationship between extreme precipitation events over EA and the various associated atmospheric circulation drivers. The analysis reveals that ECMWF-SEAS5.1 successfully reproduces the observed annual precipitation cycle and seasonal spatial pattern of rainfall over the region for both ICs, with notably better skills for September. In addition, the model effectively captures the teleconnections between EA rainfall and tropical sea surface temperature, including the Indian Ocean dipole and El Niño-Southern Oscillation, for both ICs. Regions with highest potential predictability skills coincide with regions where the model accurately represents strong (weak) composite rainfall anomalies, associated with strong (weak) moisture flux convergence (divergence) values, although the magnitude tends to be underestimated. However, other important observed features, such as the components of the African easterly jet, are well represented by the model for the September IC, but not for August. While many atmospheric mechanisms driving precipitation in the region are well simulated, their underestimation likely explains the model's general tendency to underestimate the magnitude of extreme rainfall events. The results of this study support efforts to improve forecast outputs in the national national weather services across the region by integrating ECMWF model outputs into operational weather bulletins.

**Keywords:** Equatorial Africa rainfall, Seasonal forecasting, ENSO, IOD, forecast Skill

https://doi.org/10.5194/egusphere-2025-2656
Preprint. Discussion started: 25 August 2025




## 1. Introduction

As Equatorial Africa (EA) experiences several extreme precipitation events during the September to November (SON) period (Moihamette et al., 2022; Gudoshava et al., 2022a; Kenfack et al., 2025; Nana et al., 2025), long-term seasonal precipitation forecasting is essential for effective anticipation and adaptation measures (Tanessong et al., 2017). Forecasting precipitation over the entire EA remains a persistent and complex challenge (Tanessong et al., 2013), which is far from being adequately addressed, despite advances in numerical weather and climate prediction systems. General circulation models are commonly employed by international meteorological centers for seasonal forecasts (Saha et al., 2014), and regional studies have assessed their quality at different time scales (e.g. Feudjio et al., 2022; Nana et al., 2024; Tanessong et al., 2024, 2025). However, the ability to forecast precipitation over the EA needs to be significantly enhanced to meet the growing needs of the region's populations. The inherent physical limitations of these models, which contribute to major uncertainties, often restrict their seasonal forecasting capabilities. These model-specific errors are particularly pronounced in equatorial Africa due to the sparse data density and limited understanding of the region's climate (Tanessong et al., 2017).

A number of recent investigations have provided detailed analyses of the meteorological conditions responsible for extreme flooding or drought events in EA regions and their predictability (e.g. Mwangi et al., 2014; Ehsan et al., 2022; Nana et al., 2024; Gudoshava et al., 2022b). These studies found that EA rainfall variability is mainly associated with several factors, including easterly and westerly waves, tropical cyclones, the Madden-Julian Oscillation (MJO) and sea surface temperature (SST) in the Atlantic, Indian and Pacific oceans. For example, Nana et al. (2024) demonstrated that the ability of seasonal forecast models to predict rainfall anomalies occurring over western EA during extreme South Atlantic Ocean Dipole (SAOD) events depends on their skill in forecasting the relationship between rainfall and SAOD, which decreases with increasing lead time. Their results showed that the ECMWF seasonal forecast system 5 (SEAS5) model best captures this relationship and the associated rainfall anomalies, a finding also supported by Tanessong et al. (2025). Similarly, Mwangi et al. (2014) evaluated SEAS5 products against data from ten East African stations and found significant forecasting skill for both rainy seasons, with better performance in October–December (OND) compared to March–May (MAM). The ability of the SEAS5 model to simulate the drivers of extreme rainfall during MAM 2018–2020 over eastern EA has been analyzed by Gudoshava et al. (2024). The findings of this study indicate that the heavy rainfall events of March–May 2018 and 2020 coincided with an active MJO (Phases 1–4) or a tropical cyclone east of Madagascar. In contrast, the low rainfall observed during the same period in 2019 was linked to tropical cyclones west of Madagascar. Their study also concluded that underestimation of these extreme rainfall intensities was linked to inaccurate MJO forecasts and errors in tropical cyclone location and intensity. Likewise, Tefera et al. (2025) have shown that the SEAS5 model is able (during the first two lead times) to capture the link between hydroclimatic extremes in East Africa and the co-occurrence of IOD and ENSO modes. For the June–September (JJAS) season, the findings of Ehsan et al. (2022) establish that the spatial and temporal patterns of observed EA rainfall variability, as well as the key climatic

https://doi.org/10.5194/egusphere-2025-2656
Preprint. Discussion started: 25 August 2025




features that drive EA precipitation excesses and deficits, are successfully captured by the SEAS5 model, when initialized in May and April.

During the September–November period, the equatorial Africa's rainfall system is influenced by local (Pokam et al., 2013), regional (Kuete et al., 2019; Longandjo and Rouault 2020) and large scale (Pokam et al., 2014; Nicholson 2015) factors. Among the large-scale drivers, SST variability in Pacific, Indian and Atlantic oceans plays a crucial role in interannual rainfall variability (Nicholson 2015). Motivated by this, several studies have investigated the influence of major climate modes, including ENSO (Preethi et al., 2015; Roy et al., 2024), the IOD (Palmer et al., 2023), and the South Atlantic Ocean (SAO; Nana et al., 2023). Behera et al. (2005) identify a positive relationship between rainfall anomalies over western EA and both IOD and ENSO phases. Accordingly, years marked by the simultaneous occurrence of a positive IOD and strong El Niño, such as 1997 and 2023, experienced significant heavy precipitation across East African regions (Okoola et al., 2008; Nana et al., 2025). Furthermore, Ingeri et al. (2024) found that excess rainfall over eastern EA countries (mainly Kenya, Uganda and Tanzania) is associated with positive SST anomalies over the eastern equatorial Atlantic. Over western EA, the October–November climate system is further influenced by the Indian Ocean through its teleconnection with the eastern equatorial Atlantic (Moihamette et al., 2022). Therefore, the occurrence of extreme SON rainfall events over EA likely results from the convergence of several key factors: SST anomalies in the Atlantic, Pacific and Indian oceans, the state of zonal and Walker atmospheric circulations, African Jets and the patterns of moisture transport and convergence.

This study aims to evaluate the ability of the SEAS5 version 5.1 (SEAS5.1, Johnson et al., 2019) to simulate extreme rainfall events over EA during the SON season, based on forecasts initialised in September and August. The ECMWF-SEAS5.1 model was selected in this study due to its proven ability to simulate key global climate teleconnections, including ENSO and the IOD (Nana et al., 2024; Tanessong et al., 2025), which strongly influence rainfall over Equatorial Africa (Nana et al., 2025). Its superior ability compared to other models, to reproduce regional atmospheric features (Tanessong et al., 2025) makes it a suitable choice for evaluating seasonal rainfall predictability in this region. The article is organised as follows: Section 2 details the SEAS5.1 model, the observational and reanalysis datasets, and the methodology used in this study. Section 3 presents the model skills assessment. Section 4 examines the extreme rainfall and associated SST pattern through rainfall composites, while section 5 focuses on the atmospheric circulation patterns. Finally, section 6 summarizes and concludes the paper.

## 2. Data and methods

### 2.1. SEAS5.1 re-forecast and observational datasets

In this study, we use re-forecast data from version 5.1 of the ECMWF seasonal prediction system (SEAS5.1), initiated on the 1st of September or the 1st of August for the period 1981–2016, with 25 ensemble members. Our analysis focuses on the September–November (SON) season, considering two initial conditions (ICs): September 1st (Lead-0) and August 1st (Lead-1). Monthly mean data are used throughout. To extend the study period, we include forecasts for 2017–2023, using the

https://doi.org/10.5194/egusphere-2025-2656
Preprint. Discussion started: 25 August 2025


first 25 ensemble members with the same initialization dates, ensuring each sub-period contributes equally to the analysis. This results in a total of 43 years (1981–2023), with 25 ensemble members per year. A comprehensive explanation of the ensemble generation strategy of SEAS5.1 can be found in Johnson et al. (2019). These data are available from the Copernicus Climate Data Store portal (https://climate.copernicus.eu/datasets) at a spatial resolution of 1° × 1°. The data include monthly means of total precipitation (mm day$^{-1}$), SST (K), Mean-Sea-Level Pressure (MSLP; hPa), zonal and meridional wind components (m s$^{-1}$), and specific humidity (Kg Kg$^{-1}$) at seven pressure levels (1000, 925, 850, 700, 500, 400, and 300 hPa).

As precipitation reference in this study, observed monthly precipitation data from the Climate Hazards Group Infrared Precipitation with Station data (CHIRPS; Funk et al., 2015) at 0.25° × 0.25° horizontal grid spacing are adapted. Following Dinku et al. (2018), CHIRPS has been shown to feature a good relationship with station data over eastern EA at the monthly time-scale, outperforming other satellite-based products such as Tropical Applications of Meteorology using SATellite and ground-based observations (TAMSAT) and African Rainfall Climatology version 2 (ARC2). Observed SSTs are obtained from version 5 of Extended Reconstructed SST (ERSSTv5; Huang et al., 2017) at a 2° × 2° resolution. For additional validation, we evaluate the seasonal climatologies of atmospheric circulation from SEAS5.1 against the fifth generation of European Re-Analysis (ERA5; Hersbach et al., 2020) dataset, at a horizontal (vertical) grid spacing of 0.25° × 0.25° (37 pressure levels from 1000 to 1 hPa). ERA5 was chosen based on its demonstrated ability to represent SON extreme events and their associated dynamics and thermodynamics over East Africa (Gleixner et al., 2020; Cook and Vizy, 2021). For consistency in comparison, both observed and reanalysis datasets are regridded to a 1° × 1° horizontal resolution and to seven pressure levels (1000, 925, 850, 700, 500, 400, and 300 hPa).

### 2.2. Methods

The model's Potential Predictability (PP) is estimated as the ratio between external ($\sigma_{Ext}$) and internal variance ($\sigma_{\int ¿¿}$), following the methodology of Rowell et al. (1995) and Kang and Shukla (2006). The external variance (also referred to as the signal variance) represents the variance of the ensemble mean anomalies, while internal variance (or noise variance) corresponds to the average variance of the deviations of individual ensemble members from the ensemble mean. These quantities are obtained through the following calculations:

$$\sigma_{Ext} = \frac{1}{N-1} \sum_{i=1}^{N} \left(P_i - \bar{P}\right)^2 \qquad (1)$$

$$\sigma_{Inte} = \frac{1}{N(N-1)} \sum_{i=1}^{N} \sum_{j=1}^{n} \left(P_{ij} - P_i\right)^2 \qquad (2)$$

https://doi.org/10.5194/egusphere-2025-2656
Preprint. Discussion started: 25 August 2025




$$P_i = \frac{1}{n}\sum_{j=1}^{n} P_{ij} \qquad (3)$$

$$\bar{P} = \frac{1}{Nn}\sum_{i=1}^{N}\sum_{j=1}^{n} P_{ij} \qquad (4)$$

$$PP = \frac{\sigma_{Ext}}{\sigma_{Inte}} \qquad (5)$$

where $P_{ij}$ is the model rainfall, $P_i$ is the ensemble mean for the $i$th year and $\bar{P}$ the climatology mean of all data, with i = 1, 2, …., N (N= 43, the number of years) and j = 1, 2, …., n (n= 25, the ensemble size).

This analysis uses two SST indices: the Niño 3.4 index (N34) and the Dipole Mode Index (DMI). The N34 index, used as a proxy for the ENSO, is defined as the area-averaged SST anomaly over the region 5° S–5° N, 170°–120° W (Trenberth, 1997). The DMI (Saji et al., 1999), which represents the IOD, is calculated as the difference between the area-averaged SST anomalies in the western Indian Ocean (WIO; 10° S–10° N, 50°–70° E) and the eastern Indian Ocean (EIO; 10°S-0° N, 90°–110° E).

To compute the composite anomalies, we subtract the 1981–2023 climatological mean from the composites of strong or weak events, for both the model forecasts and the observational data. To capture the variability of monthly rainfall over EA, the probability density function (PDF) based on the Gamma distribution, identified by Husak et al. (2006) as particularly appropriate for representing the asymmetric and limited nature of precipitation data, is employed. In this study, it is used to illustrate how the model, as well as the observations and reanalysis, represents the characteristics of both extreme and mean SON season rainfall over EA during the 1981–2023 period. This distribution can be expressed as follows:

$$f(P_i) = \frac{1}{\beta^{\alpha}\Gamma(\alpha)} P_i^{\alpha-1} e^{-P_i/\beta} \; for \; P_i > 0 \qquad (6)$$

where α > 0 is the shape parameter, β > 0 is the scale parameter, $P_i$ denotes the rainfall amount, and Γ(α) is the Gamma function.

Using the specific humidity (q) and horizontal wind vector (V) over the atmospheric column (1000-300 hPa), environmental conditions for extreme rainfall events are also analysed through an assessment of moisture flux convergence ∇·(qV). This quantity can be further decomposed into moisture convergence (q∇·V) and moisture advection (V·∇q), respectively, following the formulation presented by Cook and Vizy (2021) and Kolstad et al. (2024), as described by the following equation:

$$\langle \nabla \cdot (qV) \rangle = \langle q \nabla \cdot V \rangle + \langle V \cdot \nabla q \rangle \qquad (7)$$

https://doi.org/10.5194/egusphere-2025-2656
Preprint. Discussion started: 25 August 2025




where V denotes the horizontal wind and q represents the specific humidity. The angle brackets "〈〉" signify the vertical integral from the surface (1000 hPa) to the top (300 hPa) of the atmosphere column.

Based on the CHIRPS dataset, extreme SON season rainfall over EA (8°-50° E; 10° S-10° N) were identified. The EA rainfall Index (EAI) is defined by averaging the observed SON rainfall anomalies over EA and normalizing by their standard deviation. Strong (weak) years are defined as those in which the EAI is greater (less) than +1 (-1) standard deviation. Positive and negative composites analyses were then performed based on the years identified as strong and weak, respectively. Note that the same set of years was used for all observational, reanalysis, and model variables. For Pearson correlation/linear regression and composite anomaly analyses of rainfall and SST, statistical significance was determined using a standard two-tailed Student's t-test to estimate p-values. A 5% significance level was applied throughout, with results considered statistically significant if $p < 0.05$.

## 3. Model skills assessment

### 3.1. SEAS5.1 prediction of EA rainfall mean and variability

In this section, the model's ability to predict both monthly and SON season precipitation climatology is investigated. Figure 1 illustrates the annual precipitation cycle (Fig. 1a) and the precipitation fraction (Fig. 1b-d) from the CHIRPS dataset and the two lead-times of SEAS5.1. Overall, the model captures the CHIRPS annual rainfall cycle reasonably well, with a slight wet bias (0.2 to 0.6 mm day$^{-1}$) throughout the year for September IC or 0-month lead-time (L0 hereafter), except in July, similar to findings by Attada et al. (2022) over India. For August IC or 1-month lead-time (L1 hereafter), the model shows a wet bias (0.5 to 1.5 mm day$^{-1}$) from January to March and July to September, and a dry bias (0.3 to 1 mm day$^{-1}$) during April to May and November to December. At L1, the model fails to reproduce the observed rainfall peaks during March–May (MAM) and September–December (SOND) periods, unlike L0, which simulates them well. Notably, CHIRPS as well as the model at L0 both indicate rainfall peaks in April and October, while at L1, the model incorrectly shifts these peaks to March and September, respectively. During SON, the highest observed precipitation fraction (Fig. 1b) occur over the eastern part of EA (45–60 %), mainly over southern Ethiopia, eastern Kenya and Somalia, as well as over Gabon and southern Cameroon (40–45 %). Conversely, values drop below 20 % over Tanzania and northwest of Kenya. This is consistent with findings by Gudoshava et al. (2022a,b), who also showed strong (weak) rainfall contributions over southern Ethiopia, eastern Kenya and Somalia (Tanzania and northwestern Kenya). The precipitation fractions forecasted at L0 and L1 (Fig. 1c,d) align with the observed maximum percentages of total annual precipitation occurring over eastern EA, though the model underestimates (overestimates) at L0 (L1). Over western EA, SEAS5.1 slightly overestimates (underestimates) the precipitation percentage over the CB (Gabon and Equatorial Guinea) at L0, while at L1, it significantly overestimates (underestimates) rainfall contribution over southern (northern) parts of EA.

https://doi.org/10.5194/egusphere-2025-2656
Preprint. Discussion started: 25 August 2025


These results are consistent with the SON rainfall bias shown in Fig. S1a,b. At L0, the model shows a positive rainfall bias of around 3 mm day$^{-1}$ and negative rainfall bias of around -1 mm day$^{-1}$ over the CB (Gabon and Equatorial Guinea). In contrast, a larger positive bias (4 mm day$^{-1}$) in the southern region and a substantial negative bias (–4 mm day$^{-1}$) in the north are observed at L1. These findings indicate that SEAS5.1 performs better in simulating SON rainfall climatology over eastern EA, where both simulated error and absolute bias are less than 1 mm day$^{-1}$ at both lead-times (Fig. S1) compared to western EA. Furthermore, performance is generally better at L0 (bias and error around 1 mm day$^{-1}$) than at L1 (around 4 mm day$^{-1}$).

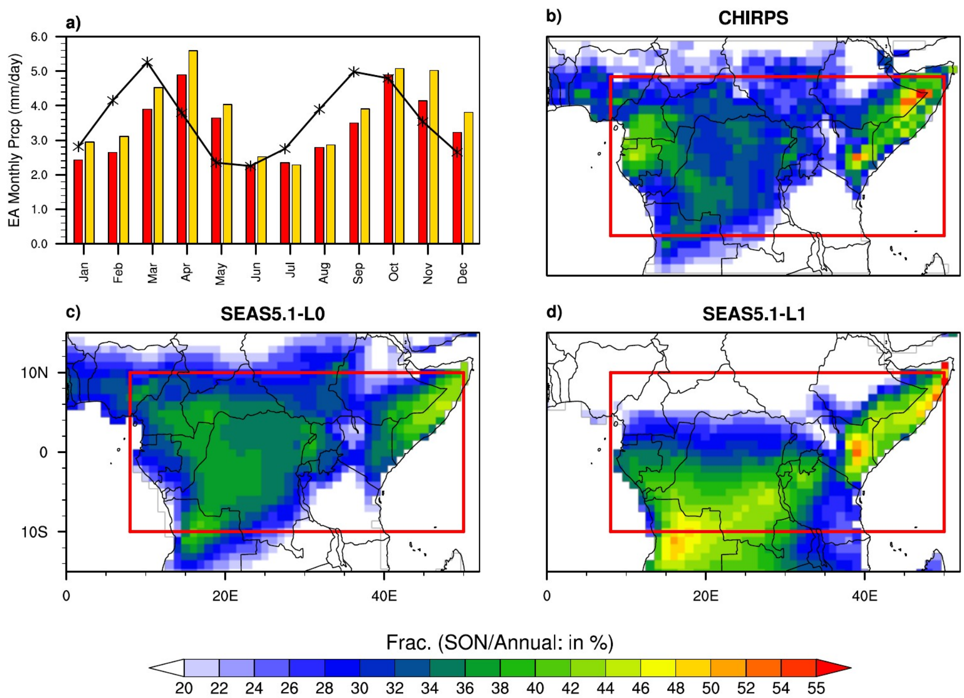


**Fig 1:** a) EA rainfall annual cycle comparing CHIRPS observation (red bar) and SEAS5.1 over the period 1981-2023. The gold bar (black line) indicates the Lead-0 (Lead-1) of the 25 ensemble members. Precipitation fraction [EA (SON/Annual, in %] for b) observation, c) Zero-month lead (Lead-0) model, and d) One-month lead (Lead-1) model. The red boxes in b), c) and d) indicate the EA boundaries.

In addition to the predicted skill assessment, the spatial distribution of the linear correlation coefficient (CC) between observed and simulated precipitation is shown in Figure 2a,b to determine the strength of SEAS5.1 to simulated SON rainfall over EA (Nana et al., 2024). The CC value varies between - 1 and 1, where values near 0 means no predictive skill, and values approaching 1 indicate good skill. At both lead-times, a large portion of EA features strong significant and positive correlations, except over the CB, Central African Republic (CAR) and southern Cameroon. These areas with

https://doi.org/10.5194/egusphere-2025-2656
Preprint. Discussion started: 25 August 2025




positive and significant (low and non-significant) correlation values coincide with areas where the model bias and RMSE values are low and even null (strong). Overall, the model skills are better at L0 compared to L1 across the region, in accord with Tefera et al. (2025) conclusion. To further investigate the relationship between observed and predicted EA precipitation, Fig. 2c,d shows the scatter plot between CHIRPS and SEAS5.1 EA rainfall at L0 (Fig. 2c) and L1 (Fig. 2d). The red lines indicate the prediction interval (PI), while green lines indicate the confidence interval (CI). At L0, the data points, as well as the PI and CI are closer to the regression line, reflecting the strong relationship shown in Fig. 2a and the low simulated errors. Notably, the CI clearly widens as precipitation values deviate from the CHIRPS mean, indicating increasing uncertainty in the true mean as we move away from the CHIRPS mean. The PI also widens, but much more than the CI for any CHIRPS value. In contrast, at L1 (Fig. 2d), the data points are more dispersed, and both the PI and CI are further away from the regression line, which is also somewhat flatter than in at L0. This finding is consistent with the low CC values observed in Fig. 2b. Similar results were reported by Ehsan et al. (2021), who also shows that the CI (linear regression line) between June-to-September Ethiopian and SEAS5 precipitation moves away from the linear regression line (bit flat) as lead-time increases.

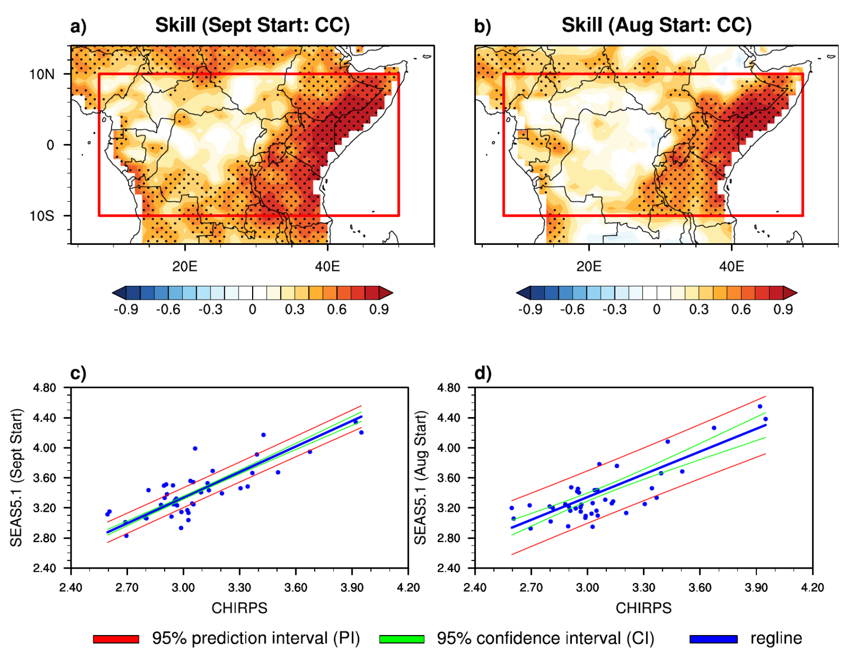


**Fig 2:** Spatial distribution of correlation coefficient (CC) between observation and ensemble mean precipitation data initialized in a) September, and b) August respectively. The stippling occurs where the correlation coefficient is statistically significant at 95% confidence level through the Student's t test. Joint plot (scatter plot) between observed (CHIRPS) and predicted (SEAS5.1) EA rainfall for c) September and d) August starts for 1981-2023. Blue line is the linear

https://doi.org/10.5194/egusphere-2025-2656
Preprint. Discussion started: 25 August 2025




regression line, red (green) lines indicate the 95% prediction (confidence) interval of the model. The red boxes in a) and b) indicate the EA boundaries.

The spatial distribution of both external (first row) and internal (second row) variances along with the ratio (third row) of these two quantities, at L0 and L1 is represented in Fig. 3. The maximum external variance values (Fig. 3a,b) occur over western and eastern parts of EA at L0, with values around 1.5 mm$^2$ day$^{-2}$ over eastern Kenya and Somalia. However, at L1, we observe a decrease in external variance, mainly over western EA, where many areas (Cameroon and Gabon) exhibit values less than 0.2 mm$^2$ day$^{-2}$. For the internal variance (Fig. 3c,d), the highest values occur at L1, and focus over Gabon, northern Angola, western Kenya and southern Tanzania. Then, the PP, as the ratio between external and internal variances is strong over coastal regions, higher at L0 (Fig. 3e) compared to L1 (Fig. 3f). These maximum values (around 3.8 at L0 and 1.3 at L1) occur where internal variance is dominated by the external variance. It is noteworthy that these high values are obtained over the tropical oceanic region (Eastern and south-western EA) where precipitation is strongly modulated by the tropical SST, in line with the findings of Kang and Shukla (2006). These analyses show that the model performs well in simulating precipitation over the region, mainly over East Africa, Gabon and the western Republic of Congo. This performance is better at L0 than at L1 (Tefera et al., 2025). However, although the model performs well in forecasting precipitation over the region during the first two lead-times, it is important to assess its ability to predict the relationship between this precipitation and its main drivers, the SSTs over the Indian and Pacific Oceans (Moihamette et al., 2022; Roy and Troccoli 2024). The following section concerns the ability of SEAS5.1 to represent the observed teleconnection.

https://doi.org/10.5194/egusphere-2025-2656
Preprint. Discussion started: 25 August 2025


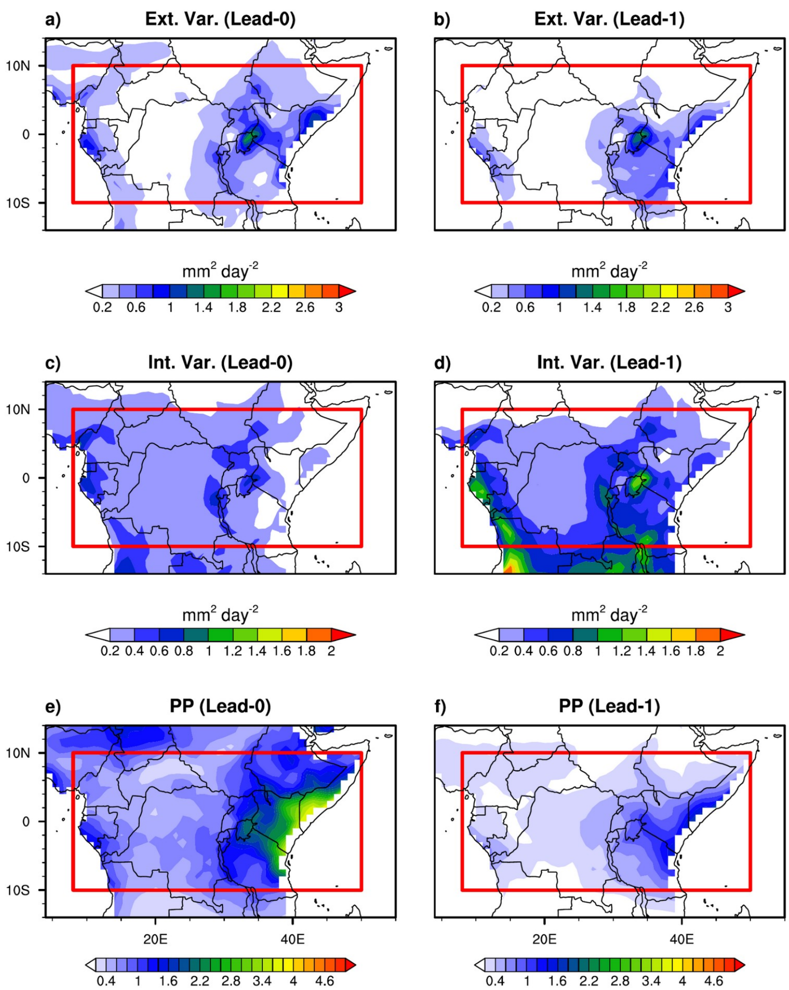


**Fig 3:** (a-b) External, (c-d) internal variances, and (e-f) PP for SON EA rainfall, for (first column) L0, and (second column) L1 respectively. The red boxes indicate the EA boundaries.

### 3.2. Physical mechanism and teleconnection patterns

https://doi.org/10.5194/egusphere-2025-2656
Preprint. Discussion started: 25 August 2025




Figure 4 shows the observed and simulated relationship through the regression analysis, between EA rainfall and the DMI. The results highlight a predominantly strong, positive and statistically significant regression between DMI and observed rainfall over the eastern part of EA (east of 30° E; Fig. 4a). Over western EA, some areas such as southern and northern DRC, and northern Angola also feature significant positive regression values. However, other regions exhibit weak (both positive and negative) and even zero regression values. These findings suggest that anomalously strong rainfall over EA is generally associated with positive IOD events, characterised by warming (cooling) of SST features over the western (eastern) pole of IOD, as mentioned by Nana et al. (2025) and Roy and Troccoli (2024). Conversely, an opposing rainfall pattern is observed during negative IOD episodes. The regression pattern between the predicted DMI and EA precipitation at L0 (Fig. 4b) and L1 (Fig. 4c) is quite similar to that observed. However, it is noteworthy that at L0, the model tends to underestimate (overestimated) the IOD teleconnection over eastern (western) EA regions, mainly Ethiopian (DRC and southern Cameroon) regression values. At L1, the positive relationship over eastern EA shifted southwards, with highest values over Tanzania and southern Kenya, where observed regression values were lower. This analysis suggests that the IOD-EA rainfall relationship is well captured in the model, which aligns with the findings of Nana et al. (2024), who point out that ECMWF is the best forecast model (among eleven predicting models) that captures SST-rainfall relationship over equatorial Africa.

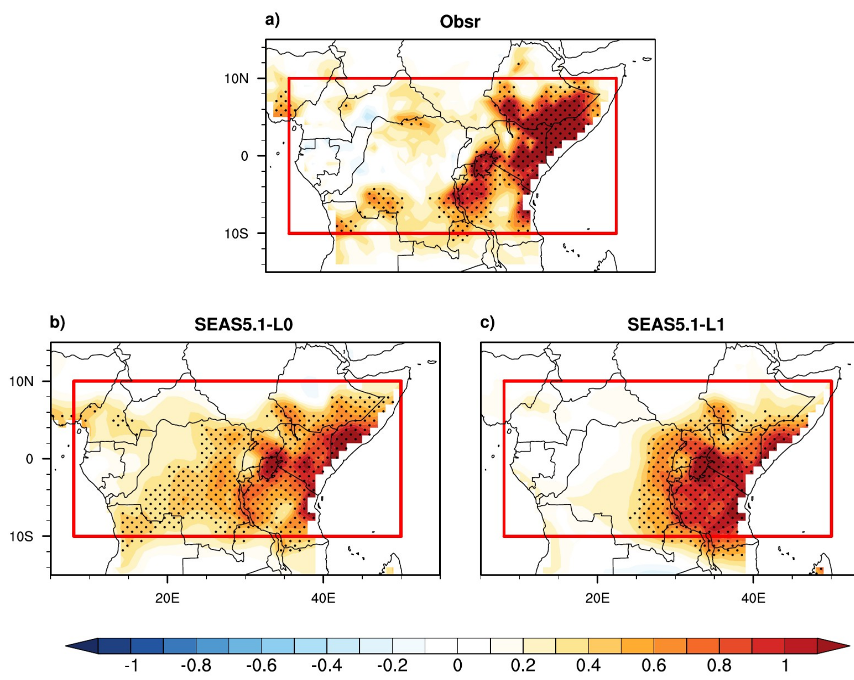

https://doi.org/10.5194/egusphere-2025-2656
Preprint. Discussion started: 25 August 2025


**Fig 4:** a) Regression of the DMI with the Precipitation during SON; (b) and (c) same as of (a) but for the SEAS5.1 dataset at L0 and L1, respectively. Stippling denotes statistical significance at 95% confidence level. The red boxes indicate the EA boundaries.

Furthermore, this regression pattern between DMI and EA rainfall remains consistent when an ENSO-type signal is present over the N34 region (Fig. 5). The results support the presence of IOD-like patterns over the IO and ENSO-like patterns over the equatorial Pacific, both in observation (Fig. 4a) and model (Fig. 4b,c). Both observed and model exhibit significant positive (negative) regression values over WIO (EIO). The equatorial Pacific highlighted here by the N3.4 index shows strong and significant positive regression, suggesting that ENSO and IOD may exert over the region a concurrent influence on rainfall distribution. This suggests that ENSO can modulate or amplify the IOD signal when both phenomena occur simultaneously. Another noteworthy pattern emerges over the eastern equatorial Atlantic, where strong positive and significant regression values are observed (Fig. 4a). Recent study by Moihamette et al. (2022) shows that rainfall variability over the areas along the Atlantic coast during IOD events can be influenced by Atlantic SST anomalies through atmospheric bridge mechanisms. The model at both L0 and L1 successfully captures this Atlantic teleconnection.

https://doi.org/10.5194/egusphere-2025-2656
Preprint. Discussion started: 25 August 2025


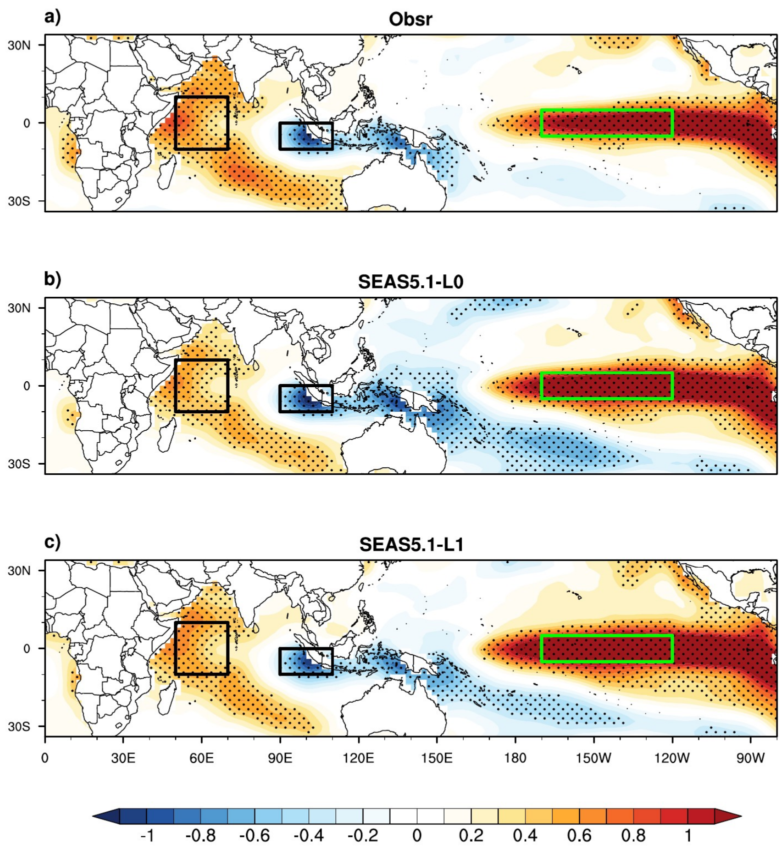


**Fig 5:** Same as Fig. 4, but for regression of the EA precipitation with the global SST. The black and green boxes indicate the IOD and N34 oceanic regions, respectively.

To further analyse the relationship between EA rainfall and both ENSO and IOD, Figure 6a outlines the scatterplots of the observed EA rainfall with the IOD and N34 indices during the SON season. The relationship between the EA rainfall index and the DMI (black triangles) as well as N34 index (red circles) is clearly positive and statistically significant (at 95% confidence level) with correlations of 0.74 and 0.40, respectively. This confirms that IOD could have an impact on the EA rainfall independently of ENSO. Moreover, these outcomes suggest that ENSO has an indirect through IOD conditions, but also a direct impact on EA precipitation through an atmospheric bridge (Ibebuchi 2021; Roy and Troccoli 2024). The SEAS5.1 captures these relationships reasonably well at both L0 and L1, but overestimated the correlations, mainly the ENSO-EA precipitation relationship (Fig. 6b,c).

https://doi.org/10.5194/egusphere-2025-2656
Preprint. Discussion started: 25 August 2025


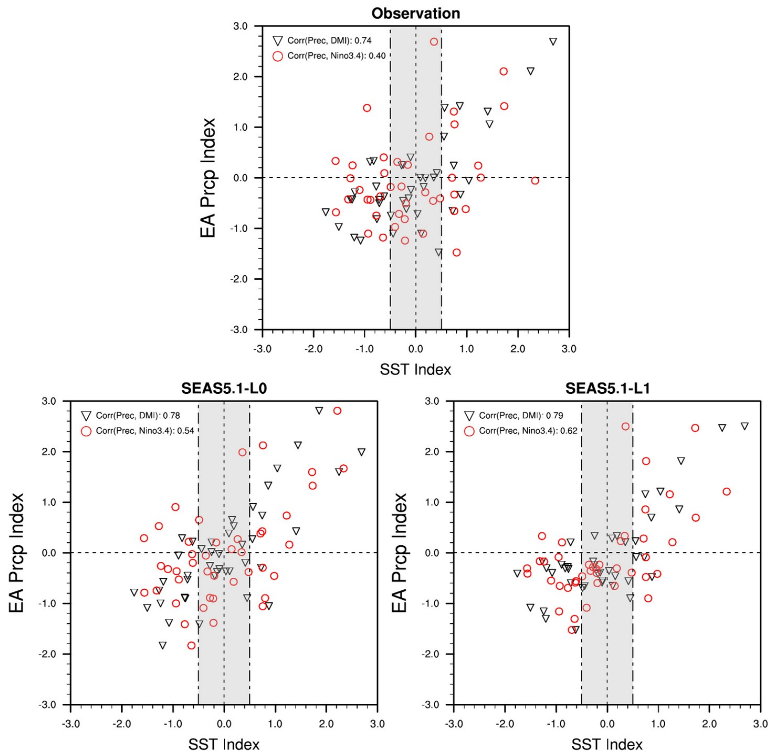


**Fig 6:** a) Observed Scatter plots for the EA precipitation with the DMI (black triangles) and N34 (red open circles) and SST based indices for the SON season. The grey shaded region corresponds to ±0.5$\sigma$ SST anomalies. Correlation Coefficient (CC) of EA precipitation index and DMI (N34) SST index is indicated at the top left of the map. (b) and (c) same as of panel (a) but for SEAS5.1 at L0 and L1, respectively.

## 3. Extreme EA rainfall: composites analysis

Firstly, we performed the time series of indices of standardised EA rainfall anomalies over the periode 1981-2023 during SON season, for CHIRPS (red bar), and SEAS5.1 at L0 (gold bar) and L1 (green bar). The CC between CHIRPS and SEAS5.1 EA rainfall index at L0 and L1 is 0.84 and 0.82, respectively (statistically significant at the 99% confidence level). The criteria used to detect extreme rainfall as described in Sect. 2.2, strong and weak EA rainfall years are defined. Thirteen extreme rainfall years have been highlighted (Fig. 7), including seven Strong Years (SY) and six Weak Years (WY). Table 1 resumes the different extreme rainfall years based on CHIRPS rainfall. Fift (three) of observed SY (WY) are captured by the model at L0, whereas four (two) are captured at L1.

https://doi.org/10.5194/egusphere-2025-2656
Preprint. Discussion started: 25 August 2025


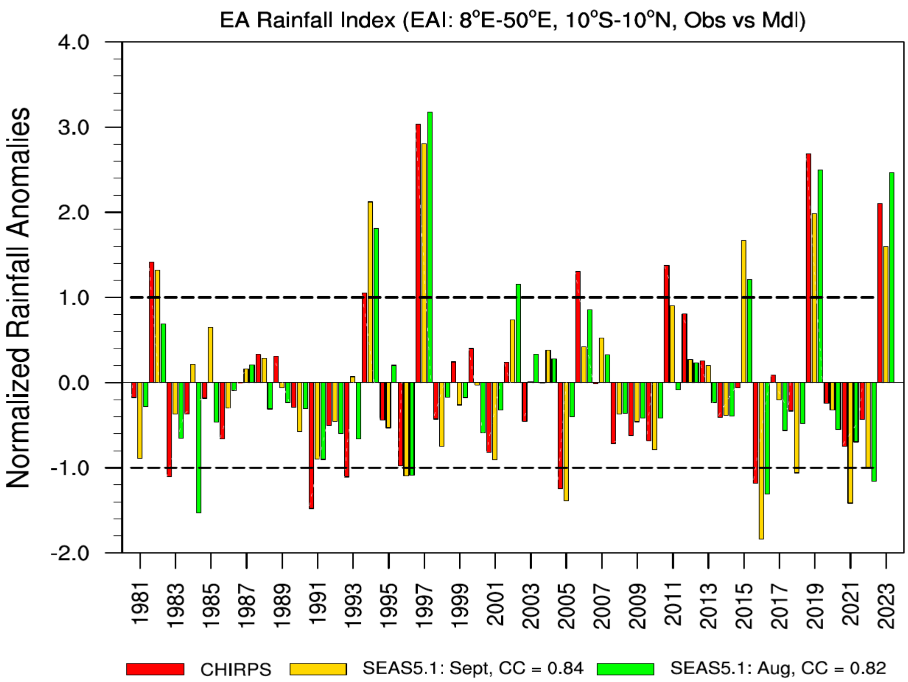


**Fig 7:** Indices of standardised EA rainfall anomalies over the periode 1981-2023 during SON, for observation (red), and model at L0 (gold) and L1 (green). Dashed black line denotes ± 1 standard deviation of seasonal anomalies. The CC value between observed and predicted EA rainfall is shown in the legend below the map.

**Table 1:** Strong and weak EA rainfall years used in this study

| Category | Years |
|---|---|
| SY | 1982*, 1994**, 1997**, 2006, 2011, 2019**, 2023** |
| WY | 1983, 1991, 1993, 1996**, 2005*, 2016** |

The asterisk (*) indicates the years capture by the model only at L0, and the double asterisk (**) those captured by the model at L0 and L1

https://doi.org/10.5194/egusphere-2025-2656
Preprint. Discussion started: 25 August 2025


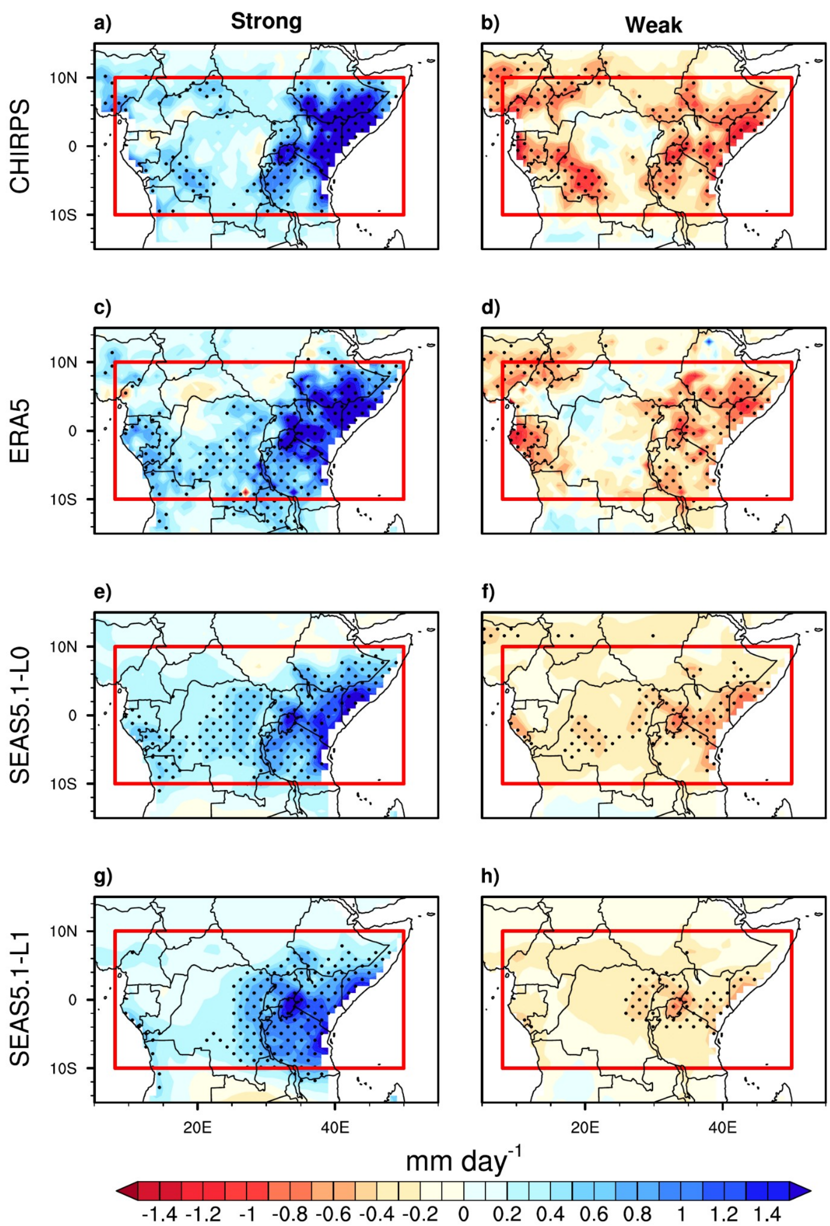


**Fig 8:** Composite of precipitation anomalies (in mm day$^{-1}$) during (first column) strong years and (weak column) weak years from (a-b) CHIRPS, (c-d) ERA5 and SEAS5.1 [L0 (e-f) and L1 (g-h)]. The red boxes indicate the EA region. The stippling occurs where the difference between the composite and the mean climatology is statistically significant at the 95% confidence level through the Student's t test

Figure 8 shows the composites of EA rainfall anomalies for SY (first column) and WY (second column). It appears that during the observed SY composites (Fig. 8a,c),

https://doi.org/10.5194/egusphere-2025-2656
Preprint. Discussion started: 25 August 2025




eastern EA experienced significant positive rainfall anomalies, mainly over southern Ethiopia and Somalia, as well as northern Kenya and Tanzania, where the IOD-rainfall relationship was strongest (Fig. 4a). Over the western EA, the positive rainfall anomalies are lower than over eastern EA, but are significant over certain areas (southwest of DRC and eastern CAR), where the IOD-rainfall relationship was strongest also. An opposite pattern is observed during the observed WY composites (Fig. 8b,d), but with a weaker (stronger) anomalies magnitude over the eastern (western) part of the EA, especially over Ethiopia, Kenya and Somalia (Cameroon, Gabon and DRC). These observed characteristics of the rainfall composites are well simulated by the model at L0 (Fig. 8e,f) as well as at L1 (Fig. 8g,f), but with a lower magnitude compared to observations (mainly during WY composites; Fig. 8f,h). During the SY composite at L1 (Fig. 8g), the northern (southern) rainfall anomalies of eastern EA are underestimated (overestimated), a similar pattern with the positive IOD-rainfall relationship over eastern EA which shifted southwards at this Lead-time (Fig. 4c).

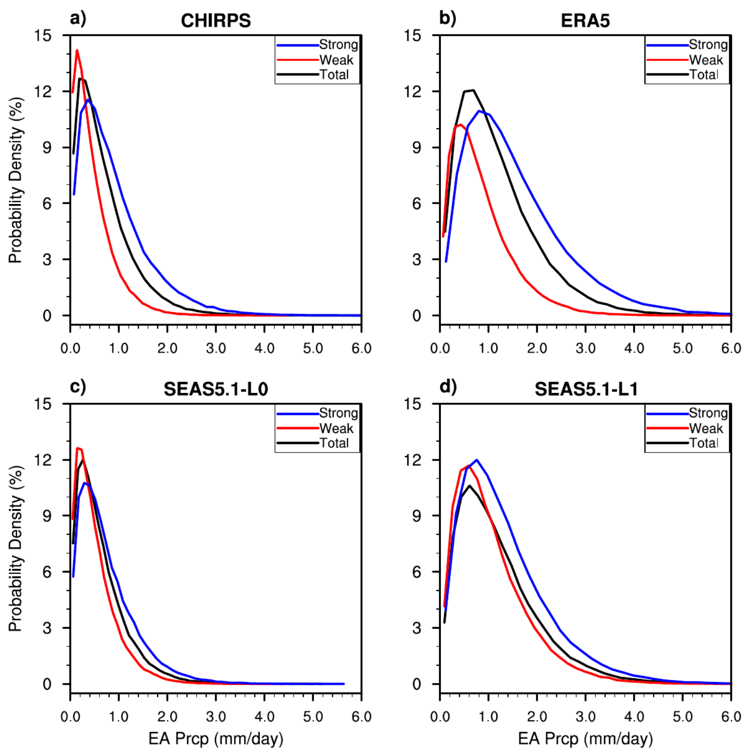


**Fig 9:** Probability Density Functions (PDFs) of SON EA precipitation from a) CHIRPS, b) ERA5, and model at c) L0 and d) L1, during the mean climatology (black line), strong years (blue line) and weak years (red line), during the period 1981-2023.

https://doi.org/10.5194/egusphere-2025-2656
Preprint. Discussion started: 25 August 2025


The monthly precipitation PDFs over EA during climatology mean (black line) SY (blue line) and WY (red line) are further investigated using gamma distribution (Fig. 9). The results confirm that more (less) observed/reanalysis rainfall are occurring over EA region during SY (WY) composites, compared to the SON mean climatology (Fig. 9a,b). These PDFs patterns were predicted successfully by SEAS5.1 at L0 (Fig. 9c) as well as at L1 (Fig. 9d).

To get an insight into the way SST responds to extreme rainfall events over EA, the composites of global SST anomalies for SY and WY events are presented in Fig. 10. As seen in Fig. 5, favourable conditions for the occurrence of EA rainfall is associated with warming (cooling) of the SST over WIO (EIO) areas (black boxes in Fig. 5), and warming of the SST over the ENSO region (green boxes in Fig. 5). It appears that during observed SY composites (Fig. 10a,c), the IO shows significant warming (cooling) of the SST located over WIO (EIO) while the area of interaction of Niño-3.4 simultaneously exhibits strong and positive SST anomalies, characterising El Niño events. An opposite pattern is observed during the WY years (Fig. 10b,d). It should be noted that the EIO exhibits stronger SST anomalies than those over the WIO, suggesting that IOD intensity is strongly modulated by the SST changes over the EIO, as suggested by Cai et al., (2011). Over the eastern equatorial Atlantic ocean, warming (cooling) SST anomalies feature during SY (WY) composites (Dezfuli and Nicholson 2013; Dezfuli 2017). These outcomes confirm that the anomalous extreme rainfall which occurs over EA during the SON season are strongly associated with SST anomalies over these three oceanic regions. The above results and conclusion are in agreement with recent findings by Nana et al. (2025). The model predicted these observed composite patterns well at L0 (Fig. 10e,f) and L1 (Fig. 10g,h). The observed SST anomalies, stronger during SY than during WY, are well simulated by the model at these two Lead-time.

https://doi.org/10.5194/egusphere-2025-2656
Preprint. Discussion started: 25 August 2025


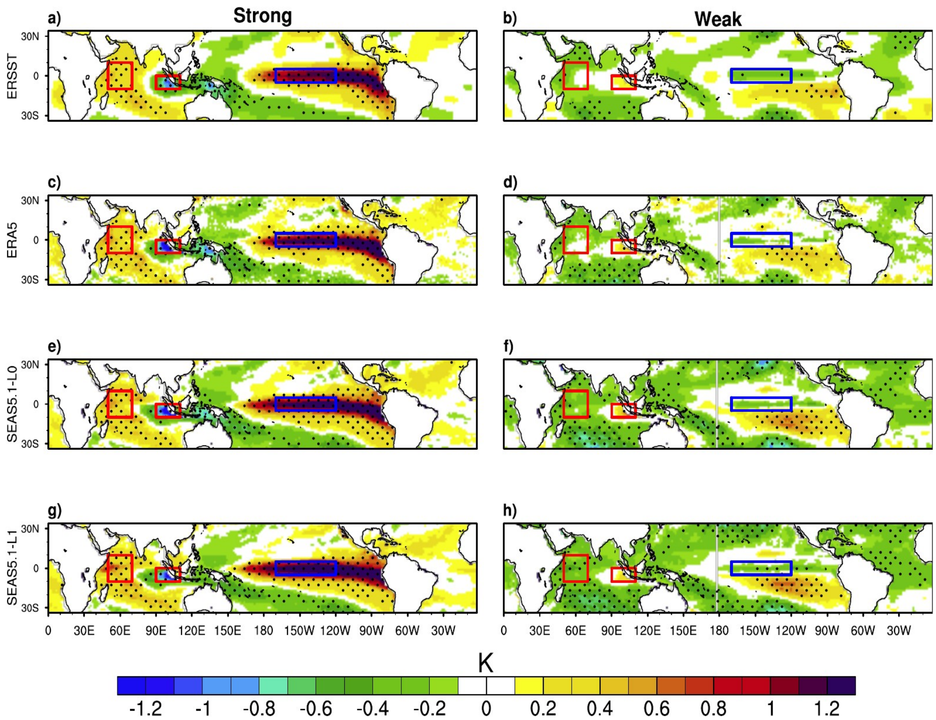


**Fig 10:** Same as in Fig. 8, but for SST (in K). The red and blue boxes indicate the IOD and N34 oceanic regions, respectively.

## 4. Atmospheric circulation: composites analysis

Previously, observed and reanalysis, as well as predicted composite SST anomalies over the Atlantic Indian, and Pacific oceans shows strong opposite pattern during both strong and weak years, which shows that EA rainfall has diverse dynamical linkages from these oceanic regions. We are now interested in the large-scale control of EA precipitation, as, following Nana et al. (2023, 2025) and Dezfuli and Nicholson (2013), interannual variations in EA precipitation are strongly influenced by large-scale climatic factors such as east Atlantic SST, IOD and ENSO. Figure 11 investigated the model's ability to predict large-scale circulation patterns through horizontal wind at 850 hPa and MSLP. During SY (WY) composites, the eastern and western equatorial IO experience strong easterly (westerly) wind anomalies, while eastern equatorial Atlantic exhibits weak westerly wind anomalies (Fig. 11a,b). According to Moihamette et al, (2022) and Nana et al. (2025), strong (weak) circulation patterns over the EA region are predominant during excess (deficit) rainfall years as a result of large-scale circulations from both equatorial Indian and eastern Atlantic oceans. These circulation patterns are associated with dipole mode over IO, more pronounced during SY (Fig. 11a) than WY (Fig. 11b), characterised by strong positive (negative) and significant values over EIO (WIO). Also, the southeast Atlantic coastal region exhibits negative composite

https://doi.org/10.5194/egusphere-2025-2656
Preprint. Discussion started: 25 August 2025


anomalies (Fig. 11a). This is consistent with the work of Dezfuli and Nicholson (2013), who found that SY (WY) events over eastern EA are associated with negative (positive) MSLP anomalies over WIO (EIO), whereas negative (positive) MSLP anomalies over southeast Atlantic coast occur during SY (WY) events over western EA. These observed composite features are well predicted with the September IC (Fig. 11c,d) and August initial condition predictions (Fig. 11e,f). The MSLP anomalies are underestimated by the model during SY (WY) at L0 (L1), mainly over WIO (whole of the EA as well as oceanic areas). These changes in SST (Fig. 10), wind and MSLP (Fig. 11) during the two rainfall events appear to be contrasted over both equatorial Atlantic and Indian oceans (strongly over the equatorial IO), and according to Pokam et al. (2012), Moihamete et al. (2022) and Nana et al. (2025), are responsible for the moisture supply over the EA during SON season.

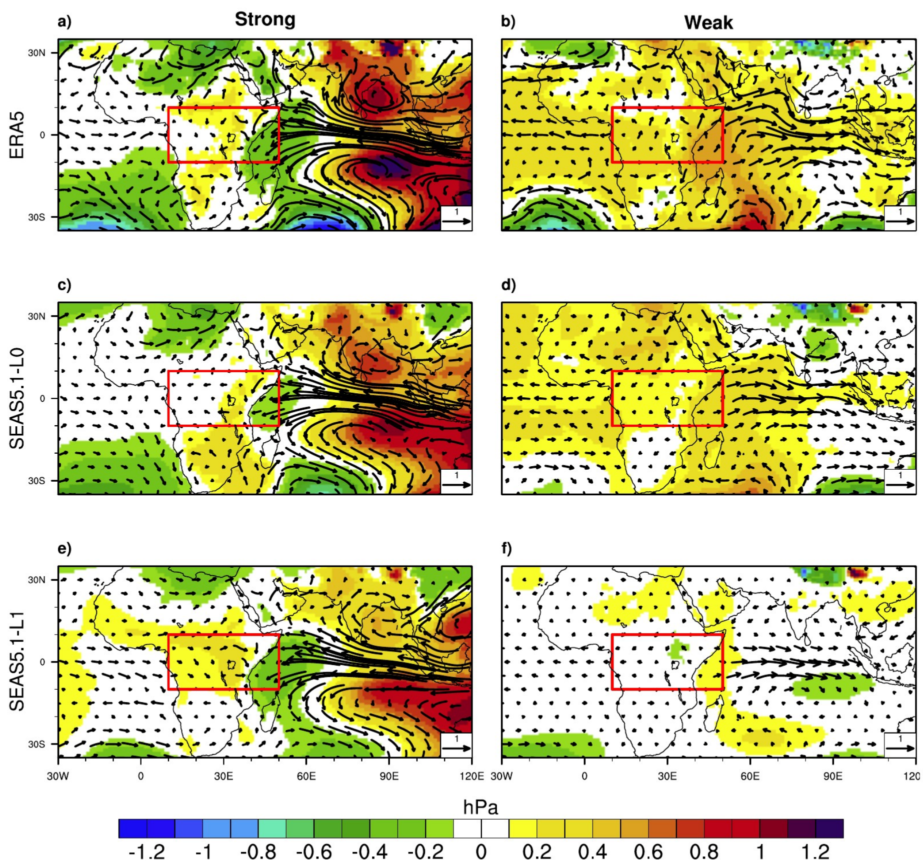


**Fig 11:** Same as in Fig. 8, but for MSLP (shading, in hPa) and 850 hPa wind (vector, m s$^{-1}$). The value higher (lower)  than 0.02 (-0.02) hPa is statistically significant at 95% confidence level

https://doi.org/10.5194/egusphere-2025-2656
Preprint. Discussion started: 25 August 2025




To highlight the atmospheric layer responsible for the moisture surplus or deficit over the region during the two extreme EA rainfall, we have examined in Figure 12 the vertical profile of the longitude-height cross-section of the observed and predicted zonal moisture flux between 1000-300 hPa, overlaid by the zonal wind and averaged between 10° S-10° N. The first column shows the SON mean climatology, the second and third column show the positive and negative composite anomalies, respectively. It emerges that the model successfully predicted the observed westerly climatology moisture transport (first column) as well as westerly wind from Atlantic Ocean to western EA in the lower troposphere (1000-850 hPa). This observed and forecast configuration in the lower troposphere over the eastern Atlantic Ocean and western EA is the same as that observed 1000-550 hPa over the Indian Ocean. However, we note an underestimate of both moisture flux and wind at L1 (Fig. 12g). During SY (second column), anomalous easterly moisture transport occurs from IO (in total troposphere) to equatorial Africa (strong over middle troposphere in the eastern part), whereas the eastern part of EA exhibited strong westerly moisture transport in the middle troposphere (850-600 hPa) from the equatorial Atlantic ocean (Fig. 12b). In the lower troposphere (1000-850 hPa), easterly moisture flows dominated over the EA region. The easterly moisture transport anomalies over IO are well captured by the model (Fig. 12e,h). However, the model overestimated (underestimated) the easterly (westerly) moisture transport over the middle troposphere (850-600 hPa) at L0 (Fig. 12e), whereas an overestimate (underestimate) of westerly (easterly) moisture transport featured over western (eastern) EA between 1000-500 hPa at L1 (Fig. 12h). During WY (third column), observation (Fig. 12c) as well as model at L0 (Fig. 12f) and L1 (Fig. 12i) shows westerly (easterly) moisture transport over the Indian (Atlantic) ocean. Over western EA domain, the model at L0 and L1 shows easterly moisture flux anomalies while observation shows westerly anomalies, but underestimated the observed Atlantic eastern moisture transport. In addition, anomalous westerly winds are weakened and easterly winds develop in the mid-troposphere (at 700 hPa), favoring equatorial easterly moisture transport. We can conclude that the two lead-time of the forecast model agree with two distinct mechanisms controlling moisture transport, over the ocean and the continent.

https://doi.org/10.5194/egusphere-2025-2656
Preprint. Discussion started: 25 August 2025


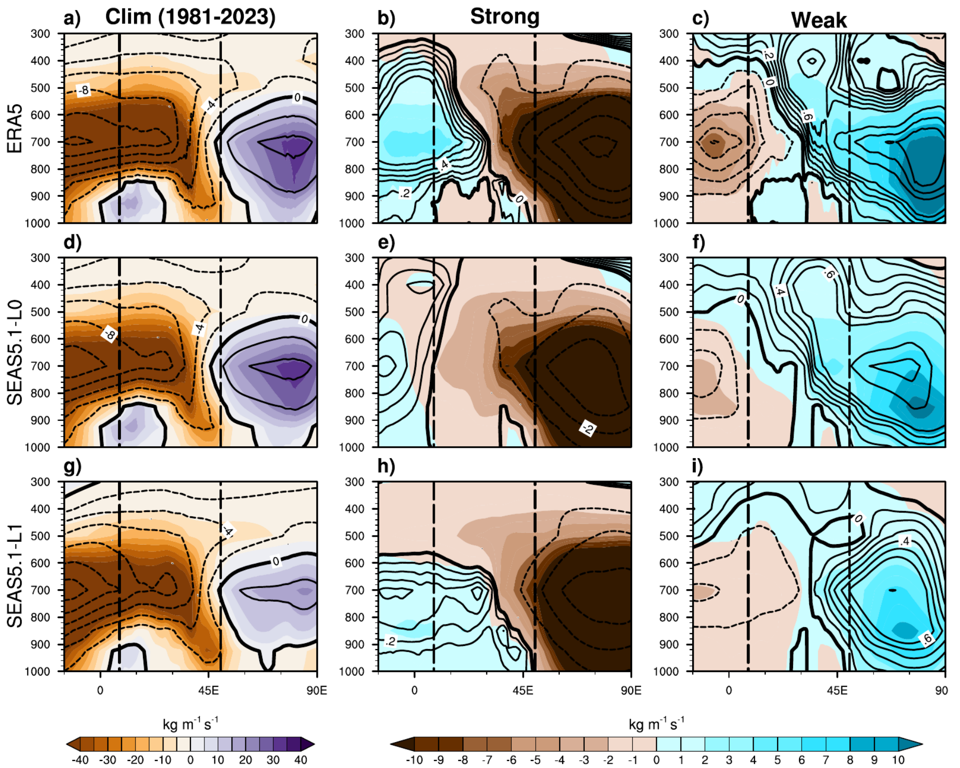


**Fig 12:** Longitude-height cross-sections for (first column) mean climatology of SON 1981-2023, (second column) strong years composite anomalies and (third column) weak years composite anomalies of zonal moisture flux (shading, kg m$^{-1}$ s$^{-1}$) and zonal wind (contour, m s$^{-1}$) for (a-c) ERA5, (d-f) L0 and (g-i) L1, averaged between 10° S-10° N. The dashed black lines denote the limits of EA.

The Figure 13 evaluated the column stratification of atmospheric convergence through the latitude/height cross-sections of the net zonal moisture flux (shading) calculated from West boundary (10° E) minus East boundary (30° E) boundary of western EA over which is overlaid the AEJ components (black dashed contours) at 15° E, and specific humidity (red contours) calculated between 10°E and 30°E. The first column shows the SON mean climatology of three tools, the second column shows the zonal moisture flux, AEJ and specific humidity composite anomaly for the SY composites, as well as the third column, but for the WY composites. The findings by Kuete et al. (2019) and Nicholson and Grist (2003) show that wet conditions over western EA are associated with decrease of the both AEJ components through increase in the middle tropospheric moisture convergence. Overall, the zonal net moisture flux balance over the EA shows a different structure for climatology and composites characterized by convergence in the middle troposphere (Fig. 13a-c) modulated by both southern and northern AEJ components, AEJ-S and AEJ-N respectively. During SY

https://doi.org/10.5194/egusphere-2025-2656
Preprint. Discussion started: 25 August 2025


(Fig. 13b) composites, the AEJ-S and AEJ-N core speed decreases compared to the climatology (Fig. 13a), leading to increases (decreases) moisture convergence (divergence) over western EA (at 10° S and 10° N boundaries of EA) favoring wet (dry) conditions, following Kuete et al. (2019) and Nicholson and Grist (2003). This middle tropospheric moisture convergence is accompanied by positive specific humidity anomalies. During WY (Fig. 13c) events, the two AEJ components are slightly stronger compared to the climatology, resulting in a strong divergence at 10° S and 10° N boundaries, and a weak mid-tropospheric convergence that contributes to intensified middle tropospheric divergence and followed by negative values of specific humidity anomalies. A similar pattern is observed at L0 (Fig. 13d-f), but slightly underestimated. Regarding the model at L1 (Fig. 13g-i), AEJ-N moves to the south, with a core speed close to 5° N versus 10° N in observation as well as L0, accompanied by a strong mid-tropospheric divergence leading to reduced mid-tropospheric convergence. Another finding is the missing of the AEJ-S in climatology and both composites.

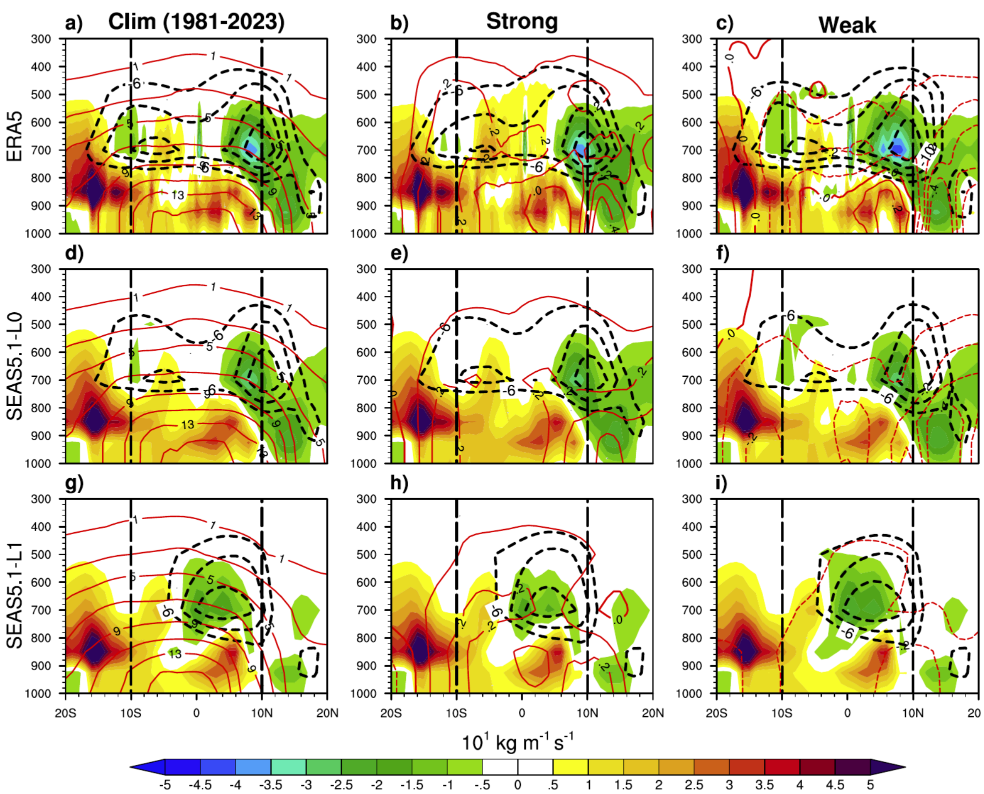


**Fig 13:** Latitude/height cross-sections of net zonal moisture flux (shading, $10^1$ kg m$^{-1}$ s$^{-1}$) calculated from West boundary (10° E) minus East boundary (30° E) for (first column) climatology of SON 1981-2023 and (second column) strong years composite anomalies and (third column) weak years composite anomalies. Black dashed lines represent AEJ components (U<-6 m s$^{-1}$) with the contour interval 2 m s$^{-1}$, calculated at 15° E for the respective periods. Red

https://doi.org/10.5194/egusphere-2025-2656
Preprint. Discussion started: 25 August 2025




solid (dashed) lines represent SON mean climatology (composite anomalies) of specific humidity with the contour interval (first column) 2 Kg Kg$^{-1}$ and (second and third column) 0.1 Kg Kg$^{-1}$, averaged over 10°-30° E for the respective periods. Positive values indicate moisture flux convergence, and negative values moisture flux divergence. The dashed black lines denote the limits of EA.

The vertically integrated moisture flux divergence (VIMFD) and vertically integrated moisture flux (VIMF) are important indicators of regions expected to receive rainfall. To provide a further exploration of the ability of ECMWF-SEAS5.1 forecasts to predict periods of heavy precipitation over the EA, we investigated the spatial patterns of both observed (Fig. 14a,b) and predicted (Fig. 14c,f) VIMFD anomalies over 1000-300 hPa during SY and WY composites. SY (Fig. 14a) composite is characterised by an anomalous VIMF associated with easterly and westerly flux over WIO and eastern equatorial Atlantic, respectively. This moisture advection extends across the EA with anomalous strong moisture convergence leading to wetter conditions over the region, with highest moisture convergence anomaly values occurring over the eastern EA. An opposite pattern feature during WY composite (Fig. 14b). Although underestimated, the observed pattern is well predicted by the model at L0 (Fig. 14c-d) and L1 (Fig. 14e-f). Furthermore, examination of Figures S2 and S3 confirms that moisture convergence is the main component of moisture flux convergence, since, the spatial pattern of moisture convergence ($q\nabla \cdot V$) is similar (and with the same strengths) to that of moisture flux convergence ($\nabla \cdot (qV)$), in contrast to that of moisture advection ($V \cdot \nabla q$). This finding is in line with previous research by Longandjo and Rouault (2023) and Kolstad et al. (2024), who show that moisture convergence prevails in moisture flux convergence over western EA and eastern EA, respectively. The model captures this moisture convergence very well as the main component of moisture flux convergence (Kolstad et al. 2024) at L0 (Figs. S2c,d and Figs. S3c,d) and L1 (Figs. S2e,f and Figs. S3e,f). We therefore conclude that the physical mechanisms that generate precipitation in the prediction data for the IC of September and August are reasonable, and that it is appropriate to use the SEAS5.1 prediction outputs for precipitation over the EA.

https://doi.org/10.5194/egusphere-2025-2656
Preprint. Discussion started: 25 August 2025


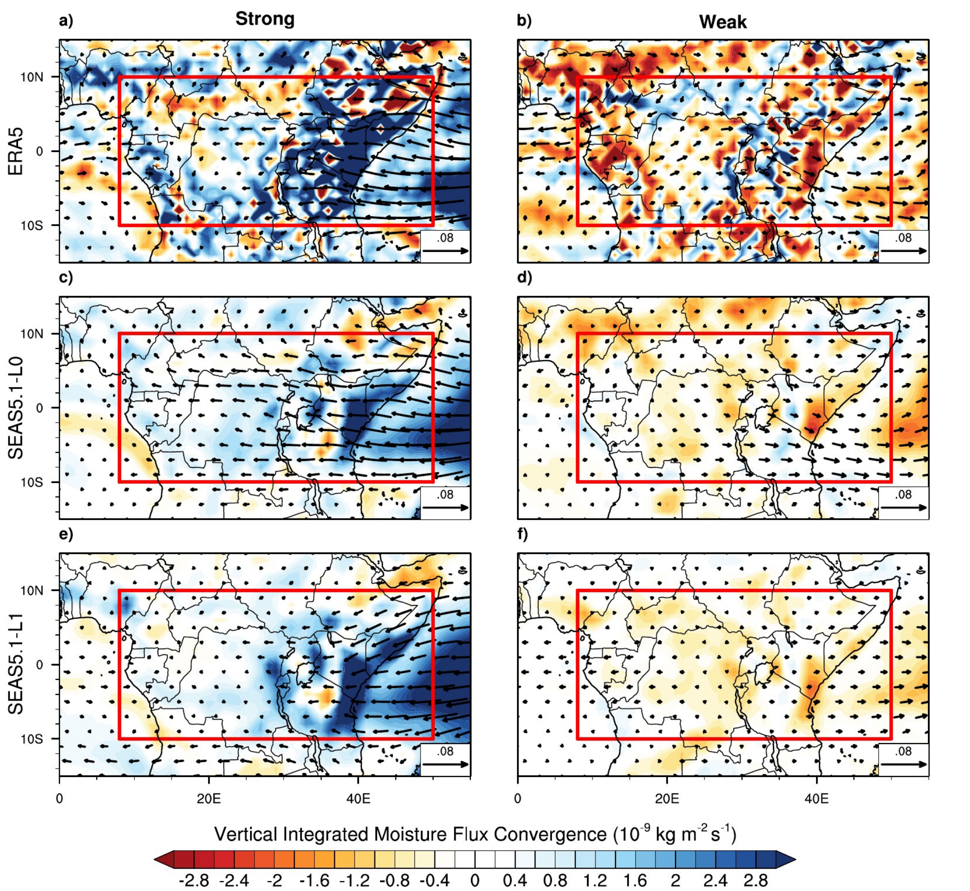


**Fig 14:** Same as Fig. 8, but for vertically integrated (1000-300 hPa) moisture flux (vectors, $10^{-9}$ kg $m^{-1}$ $s^{-1}$) and vertically integrated moisture flux convergence (positive values) or divergence (negative values) anomalies (shading, $10^{-6}$ kg $m^{-2}$ $s^{-1}$). Only significant vectors and shading above the 90 % level are shown. The red box indicates the EA region.

## 5. Summary and conclusions

By analysing hindcast and forecast from the latest operational seasonal forecasting system based on dynamical climate models, the European Centre for Medium-Range Weather Forecasts seasonal prediction system 5, version 5.1 (ECMWF-SEAS5.1), this study highlights the influence of atmospheric drivers in forecasting extreme precipitation events over equatorial Africa (EA) during the September-October-November (SON) season for the period 1981–2023 (43 years). While some anomalous rainfall patterns over eastern and western EA have been linked to moisture transport from the Indian and Atlantic oceans respectively, further investigation is needed to evaluate the model's ability to simulate the Madden–Julian Oscillation (MJO)

https://doi.org/10.5194/egusphere-2025-2656
Preprint. Discussion started: 25 August 2025


activity during these extreme events. The key findings of this study are summarized as follows:

- The spatiotemporal and interannual variability of EA rainfall is well represented by ECMWF-SEAS5.1 in both lead times during the SON season.
- The ECMWF-SEAS5.1 model exhibits low skill in predicting rainfall over the Congo Basin in both hindcasts. At L0, the data points are more dispersed than at L1, and both the prediction and confidence intervals lie farther from the regression line, which is slightly flatter compared to L1.
- Potential Predictability skill is generally higher for the short lead-time (September IC) when considering the entire equatorial Africa domain. However, for the longer lead-time (August IC), a larger number of grid points in the eastern EA exhibit high correlation values, reaching up to 0.7.
- ECMWF-SEAS5.1 successfully captures the large-scale teleconnection between tropical SST over the Atlantic, Indian and Pacific oceans and precipitation over EA, with forecasts initialized in September (Lead-0) showing higher teleconnection skill compared to those initialized in August (Lead-1).
- For the September IC, the model captures 71.4 % of the observed strong years and 50.0 % of weak years, while for the August IC, it captured 57.1 % of strong years and 33.3 % of weak years.
- The ECMWF-SEAS5.1 model successfully captures the maximum composite rainfall anomalies over eastern EA, mainly over the whole of Kenya, southern Ethiopia and Somalia, although it tends to underestimate the magnitude. Performance is better for September initial conditions compared to August.
- Similarly, both the IOD and ENSO modes are well simulated during extreme events, as well as for both lead times, along with the atmospheric circulation associated with these oceanic modes.
- The ECMWF-SEAS5.1 model successfully simulates moisture flux convergence and its two components (moisture convergence and moisture advection) with relatively better skill for September IC compared to August.

This study demonstrates that the novel ECMWF-SEAS5 version 5.1 (SEAS5.1) outperforms its predecessors (ECMWF-SEAS5 version 5; Nana et al., 2024 and Tanessong et al., 2025), and exhibits strong and statistically significant skill in capturing the atmospheric characteristics associated with extreme rainfall events over EA. Given that skillful seasonal forecasting of equatorial rainfall has critical social and economic impacts, notably the ability to restock reservoirs and recharge groundwater, which have greatly improved irrigation planning, and enhanced agricultural productivity, these findings offer valuable insights for policy-makers in the region to make informed decisions on adaptation strategies and risk mitigation.

https://doi.org/10.5194/egusphere-2025-2656
Preprint. Discussion started: 25 August 2025


**Acknowledgements** The authors thank you to all reanalysis, observational, satellite and hindcast data providers used in this study. We would like to express our gratitude to the anonymous reviewers, along with the editor for their constructive suggestions, which have greatly improved the quality of the paper. We gratefully appreciate the efforts of the International Joint Laboratory Dynamics of Terrestrial Ecosystems in Central Africa (IJL DYCOCA/ LMI DYCOFAC) initiative during the realisation of this work.

**Code availability** Figures shown in this study are plotted using the NCAR Command Language (NCL; https://doi.org/10.5065/D6WD3XH5, NCAR Command Language, 2017). Codes can be obtained from the corresponding author.

**Author's contributions HNN**: Conceptualization; data upload; data analysis; formal analysis; investigation; methodology; software; validation; writing-original draft; writing-review and editing. **RST:** Project administration; supervision; validation; methodology; writing; review and editing. **MG:** Investigation; validation; writing-original draft; writing-review and editing. **DAV:** Project administration; supervision; validation, methodology; writing; review and editing.

**Funding** Not applicable

**Data availability** All observational and reanalysis data used in this study are publicly available at no charge and with unrestricted access. The ERA5 reanalysis is produced within the Copernicus Climate Change Service (C3S) by the ECMWF and is accessible via the link https://cds.climate.copernicus.eu/datasets/; the CHIRPS2 data are available at https://data.chc.ucsb.edu/products/CHIRPS-2.0/global_daily/netcdf/; the ERSST data are available at https://iridl.ldeo.columbia.edu/SOURCES/.NOAA/.NCDC/.ERSST/.version5/. The ECMWF-SEAS5.1 model data can be downloaded from the Copernicus Climate Data Store (https://cds.climate.copernicus.eu/datasets/seasonal-monthly-pressure-levels?tab=download)

**Conflict of interest** The authors declare no conflicts of interest relevant to this study.

https://doi.org/10.5194/egusphere-2025-2656
Preprint. Discussion started: 25 August 2025


**References**

Attada, R., Ehsan, M. A., and Pillai, P. A.: Evaluation of potential predictability of indian summer monsoon rainfall in ecmwf's fifth-generation seasonal forecast system (SEAS5), Pure Appl. Geophys., 179, 4639–4655, https://doi.org/10.1007/s00024-022-03184-9, 2022.

Behera, S. K., Luo, J.-J., Masson, S., Delecluse, P., Gualdi, S., Navarra, A., and Yamagata, T.: Paramount impact of the Indian Ocean dipole on the East African short rains: A CGCM study, J. Climate, 18, 4514–4530, https://doi.org/10.1175/jcli3541.1, 2005.

Cai, W., van Rensch, P., Cowan, T., and Hendon, H. H.: Teleconnection pathways of ENSO and the IOD and the mechanisms for impacts on australian rainfall, J. Climate, 24, 3910–3923, https://doi.org/10.1175/2011jcli4129.1, 2011.

Cook, K. H. and Vizy, E. K.: Hydrodynamics of regional and seasonal variations in Congo Basin precipitation, Clim. Dynam., 59, 1775–1797, https://doi.org/10.1007/s00382-021-06066-3, 2021.

Dezfuli, A.: Climate of Western and Central Equatorial Africa. In Oxford Research Encyclopedia of Climate Science. Oxford University Press. https://doi.org/10.1093/acrefore/9780190228620.013.511, 2017.

Dezfuli, A. K. and Nicholson, S. E.: The relationship of rainfall variability in Western Equatorial Africa to the tropical oceans and atmospheric circulation. Part II: The Boreal Autumn, J. Climate, 26, 66–84, https://doi.org/10.1175/jcli-d-11-00686.1, 2013.

Dinku, T., Funk, C., Peterson, P., Maidment, R., Tadesse, T., Gadain, H., and Ceccato, P.: Validation of the CHIRPS satellite rainfall estimates over eastern Africa, Quart. J. Roy. Meteorol. Soc., 144, 292–312, https://doi.org/10.1002/qj.3244, 2018.

Ehsan, M. A., Tippett, M. K., Robertson, A. W., Almazroui, M., Ismail, M., Dinku, T., Acharya, N., Siebert, A., Ahmed, J. S., and Teshome, A.: Seasonal predictability of Ethiopian Kiremt rainfall and forecast skill of ECMWF's SEAS5 model, Clim. Dynam., 57, 3075–3091, https://doi.org/10.1007/s00382-021-05855-0, 2021.

Feudjio Tchinda, A., Tanessong, R. S., Mamadou, O., Tchida Diffo, V., Djomou Yepdo, Z., and Chabi Orou, J. B.; Predictive skill of North American Multi-Model Ensemble seasonal forecasts for the climate rainfall over Central Africa, Meterol. Appl., 29, https://doi.org/10.1002/met.2074, 2022.

Funk, C., Peterson, P., Landsfeld, M., Pedreros, D., Verdin, J., Shukla, S., Husak, G., Rowland, J., Harrison, L., Hoell, A., and Michaelsen, J.: The climate hazards infrared precipitation with stations—a new environmental record for monitoring extremes, Sci. Data, 2, https://doi.org/10.1038/sdata.2015.66, 2015.

Gleixner, S., Demissie, T., and Diro, G. T.: Did ERA5 improve temperature and precipitation reanalysis over east africa, Atmosphere, 11, 996. https://doi.org/10.3390/atmos11090996, 2020.

https://doi.org/10.5194/egusphere-2025-2656
Preprint. Discussion started: 25 August 2025


Gudoshava, M., Nyinguro, P., Talib, J., Wainwright, C., Mwanthi, A., Hirons, L., de Andrade, F., Mutemi, J., Gitau, W., Thompson, E., Gacheru, J., Marsham, J., Endris, H. S., Woolnough, S., Segele, Z., Atheru, Z., and Artan, G.: Drivers of sub-seasonal extreme rainfall and their representation in ECMWF forecasts during the Eastern African March-to-May seasons of 2018–2020, Meterol. Appl., 31, https://doi.org/10.1002/met.70000, 2024.

Gudoshava, M., Wainwright, C., Hirons, L., Endris, H. S., Segele, Z. T., Woolnough, S., Atheru, Z., and Artan, G.: Atmospheric and oceanic conditions associated with early and late onset for Eastern Africa short rains, Int. J. Climatol., 42, 6562–6578, https://doi.org/10.1002/joc.7627, 2022.

Gudoshava, M., Wanzala, M., Thompson, E., Mwesigwa, J., Endris, H. S., Segele, Z., Hirons, L., Kipkogei, O., Mumbua, C., Njoka, W., Baraibar, M., de Andrade, F., Woolnough, S., Atheru, Z., and Artan, G.: Application of real time S2S forecasts over Eastern Africa in the co-production of climate services, Clim. Serv., 27, 100319, https://doi.org/10.1016/j.cliser.2022.100319, 2022.

Hersbach, H., Bell, B., Berrisford, P., Hirahara, S., Horányi, A., Muñoz-Sabater, J., Nicolas, J., Peubey, C., Radu, R., Schepers, D., Simmons, A., Soci, C., Abdalla, S., Abellan, X., Balsamo, G., Bechtold, P., Biavati, G., Bidlot, J., Bonavita, M., ... Thépaut, J.: The ERA5 global reanalysis, Quart. J. Roy. Meteorol. Soc., 146, 1999–2049, https://doi.org/10.1002/qj.3803, 2020.

Huang, B., Thorne, P. W., Banzon, V. F., Boyer, T., Chepurin, G., Lawrimore, J. H., Menne, M. J., Smith, T. M., Vose, R. S., and Zhang, H.-M.: Extended reconstructed sea surface temperature, version 5 (ersstv5): Upgrades, validations, and intercomparisons, J. Climate, 30, 8179–8205, https://doi.org/10.1175/jcli-d-16-0836.1, 2017.

Husak, G. J., Michaelsen, J., and Funk, C.: Use of the gamma distribution to represent monthly rainfall in Africa for drought monitoring applications, Int. J. Climatol., 27, 935–944, https://doi.org/10.1002/joc.1441, 2006.

Ibebuchi, C. C.: Revisiting the 1992 severe drought episode in South Africa: The role of El Niño in the anomalies of atmospheric circulation types in Africa south of the equator, Theor. Appl. Climatol., 146, 723–740, https://doi.org/10.1007/s00704-021-03741-7, 2021.

Ingeri, C., Wen, W., Sebaziga, J. N., Iyakaremye, V., Ekwacu, S., Ayabagabo, P., Twahirwa, A., and Kazora, J.: Potential driving systems associated with extreme rainfall across East Africa during october to december (OND) season 2019, J. Geosci. Environ. Prot., 12, 25–49, https://doi.org/10.4236/gep.2024.127003, 2024.

Johnson, S. J., Stockdale, T. N., Ferranti, L., Balmaseda, M. A., Molteni, F., Magnusson, L., Tietsche, S., Decremer, D., Weisheimer, A., Balsamo, G., Keeley, S. P. E., Mogensen, K., Zuo, H., and Monge-Sanz, B. M.: SEAS5: The new ECMWF

https://doi.org/10.5194/egusphere-2025-2656
Preprint. Discussion started: 25 August 2025


seasonal forecast system, Geosci. Model Dev., 12, 1087–1117, https://doi.org/10.5194/gmd-12-1087-2019, 2019.

Kang, I.-S., and Shukla, J.: Dynamic seasonal prediction and predictability of the monsoon, In: Wang B (ed) The Asian Monsoon. Praxis. Springer, Berlin Heidelberg, pp 585– 612, https://doi.org/10.1007/3-540-37722-0_15, 2006.

Kenfack, K., Marra, F., Djomou, Z. Y., Tchotchou, L. A. D., Tamoffo, A. T., and Vondou, D. A.: Dynamic and thermodynamic contribution to the October 2019 exceptional rainfall in western central Africa, Weather Clim. Dynam., 5, 1457–1472, https://doi.org/10.5194/wcd-5-1457-2024, 2024.

Kolstad, E. W., and MacLeod, D.: Lagged oceanic effects on the East African short rains, Clim.Dynam., 59, 1043–1056, https://doi.org/10.1007/s00382-022-06176-6, 2022.

Kolstad, E. W., Parker, D. J., MacLeod, D. A., Wainwright, C. M., and Hirons, L. C.: Beyond the regional average: Drivers of geographical rainfall variability during East Africa's short rains, Quart. J. Roy. Meteorol. Soc., 150, 4550–4566, https://doi.org/10.1002/qj.4829, 2024.

Kuete, G., Pokam Mba, W., and Washington, R.: African Easterly Jet South: Control, maintenance mechanisms and link with Southern subtropical waves, Clim. Dynam., 54, 1539–1552. https://doi.org/10.1007/s00382-019-05072-w, 2019.

Longandjo, G.-N. T., and Rouault, M.: On the structure of the regional-scale circulation over Central Africa: Seasonal evolution, variability, and mechanisms, J. Climate, 33, 145–162, https://doi.org/10.1175/jcli-d-19-0176.1, 2020.

Longandjo, G.-N. T., and Rouault, M.: Revisiting the seasonal cycle of rainfall over Central Africa. Research Square Platform LLC, https://doi.org/10.21203/rs.3.rs-2956778/v1, 2023.

Moihamette, F., Pokam, W. M., Diallo, I., and Washington, R.: Extreme Indian Ocean dipole and rainfall variability over Central Africa, Int. J. Climatol., 42, 5255–5272, https://doi.org/10.1002/joc.7531, 2022.

Mwangi, E., Wetterhall, F., Dutra, E., Di Giuseppe, F., and Pappenberger, F.: Forecasting droughts in East Africa, Hydrol. and Earth Syst. Sci., 18, 611–620, https://doi.org/10.5194/hess-18-611-2014, 2014.

Nana, H. N., Gudoshava, M., Tanessong, R. S., Tamoffo, A. T., & Vondou, D. A. (2025). Diverse causes of extreme rainfall in november 2023 over equatorial africa. Copernicus GmbH. https://doi.org/10.5194/egusphere-2025-76

Nana, H. N., Tamoffo, A. T., Kaissassou, S., Djiotang Tchotchou, L. A., Tanessong, R. S., Kamsu-Tamo, P. H., Kenfack, K., and Vondou, D. A.: Performance-based evaluation of NMME and C3S models in forecasting the June–August Central African rainfall under the influence of the South Atlantic Ocean Dipole, Int. J. Climatol., 44, 2462–2483, https://doi.org/10.1002/joc.8463, 2024.

Nana, H. N., Tanessong, R. S., Tchotchou, L. A. D., Tamoffo, A. T., Moihamette, F., and Vondou, D. A.: Influence of strong South Atlantic Ocean Dipole on the Central African rainfall's system, Clim. Dynam., 62 1–16,

https://doi.org/10.5194/egusphere-2025-2656
Preprint. Discussion started: 25 August 2025




https://doi.org/10.1007/s00382-023-06892-7, 2023.

Nicholson, S. E.: Long-term variability of the East African 'short rains' and its links to large- scale factors, Int. J. Climatol., 35, 3979–3990, https://doi.org/10.1002/joc.4259, 2015.

Nicholson, S. E., and Grist, J. P.: The seasonal evolution of the atmospheric circulation over west africa and equatorial africa, J. Climate, 16, 1013–1030, https://doi.org/10.1175/1520-0442(2003)016<1013:tseota>2.0.co;2, 2003.

Okoola R. E., Camberlin P., Ininda J. M.: Wet periods along the East African Coast and the extreme wet spell of October 1997, J. Kenya Meteorol., Soc 2:67–83, 2008.

Palmer, P. I., Wainwright, C. M., Dong, B., Maidment, R. I., Wheeler, K. G., Gedney, N., Hickman, J. E., Madani, N., Folwell, S. S., Abdo, G., Allan, R. P., Black, E. C. L., Feng, L., Gudoshava, M., Haines, K., Huntingford, C., Kilavi, M., Lunt, M. F., Shaaban, A., and Turner, A. G.: Drivers and impacts of Eastern African rainfall variability, Nat. Rev. Earth Environ., 4, 254–270, https://doi.org/10.1038/s43017-023-00397-x, 2023.

Pokam, W. M., Bain, C. L., Chadwick, R. S., Graham, R., Sonwa, D. J., and Kamga, F. M.: Identification of processes driving low-level westerlies in west equatorial africa, J. Climate, 27, 4245–4262, https://doi.org/10.1175/jcli-d-13-00490.1, 2014.

Pokam, W. M., Djiotang, L. A. T., and Mkankam, F. K.: Erratum to: Atmospheric water vapor transport and recycling in Equatorial Central Africa through NCEP/NCAR reanalysis data, Clim. Dynam., 42, 553–553, https://doi.org/10.1007/s00382-013-1977-4, 2013.

Preethi, B., Sabin, T. P., Adedoyin, J. A., and Ashok, K.: Impacts of the ENSO Modoki and other Tropical Indo-Pacific Climate-Drivers on African Rainfall, Sci. Rep., 5, https://doi.org/10.1038/srep16653, 2015.

Rowell, D. P., Folland, C. K., Maskell, K., and Ward, N. M.: Variability of summer rainfall over tropical north Africa (1906-92): Observations and modelling, Quart. J. Roy. Meteorol. Soc., 121, 669–704, https://doi.org/10.1256/smsqj.52310, 1995.

Roy, I., and Troccoli, A.: Identifying important drivers of East African October to December rainfall season, Sci. Tot. Env., 914, 169615, https://doi.org/10.1016/j.scitotenv.2023.169615, 2024.

Saha, S., Moorthi, S., Wu, X., Wang, J., Nadiga, S., Tripp, P., Behringer, D., Hou, Y.-T., Chuang, H., Iredell, M., Ek, M., Meng, J., Yang, R., Mendez, M. P., van den Dool, H., Zhang, Q., Wang, W., Chen, M., and Becker, E.: The NCEP climate forecast system version 2, J. Climate, 27, 2185–2208, https://doi.org/10.1175/jcli-d-12-00823.1, 2014.

Saji, N. H., Goswami, B. N., Vinayachandran, P. N., and Yamagata, T.: A dipole mode in the tropical Indian Ocean, Nature, 401, 360–363, https://doi.org/10.1038/43854, 1999.

Tanessong, R. S., Fotso-Nguemo, T. C., Kaissassou, S., Guenang, G. M., Komkoua Mbienda, A. J., Djiotang Tchotchou, L. A., Tchinda, A. F., Vondou, D. A., Pokam, W. M., Igri, P. M., and Yepdo, Z. D.: Climate forecast skill and teleconnections on seasonal time scales over Central Africa based on the North American Multi-Model Ensemble (NMME), Meteorol. Atmos. Phys., 136, https://doi.org/10.1007/s00703-024-01018-y, 2024.

Tanessong, R. S., Igri, P. M., Vondou, D. A., Tamo, P. H. K., and Kamga, F. M.: Evaluation of probabilistic precipitation forecast determined from WRF forecasted amounts, Theor. Appl. Climatol., 116, 649–659, https://doi.org/10.1007/s00704-013-0965-2, 2013.

Tanessong, R. S., Vondou, D. A., Djomou, Z. Y., and Igri, P. M.: WRF high resolution simulation of an extreme rainfall event over Douala (Cameroon): A case study, Model. Earth Syst. Environ., 3, 927–942, https://doi.org/10.1007/s40808-017-0343-7, 2017.

Tefera, A. K., Liguori, G., Cabos, W., and Navarra, A.: Seasonal forecasting of East African short rains, Sci. Rep., 15, https://doi.org/10.1038/s41598-025-86564-0, 2025.

Trenberth, K. E.: The definition of El Niño, Bull. Amer. Meteorol. Soc., 78, 2771–2777, https://doi.org/10.1175/1520-0477(1997)078<2771:tdoeno>2.0.co;2, 1997.